NOTES AND CORRESPONDENCE

The Conservation of Potential Vorticity along Lagrangian Trajectories in Simulations of Eddy-Driven Flows

BACH LIEN HUA

Laboratoire de Physique des Oceans, IFREMER, Plouzané, France

2 August 1992 and 19 May 1993

ABSTRACT

The purpose of this note is to investigate the use of Lagrangian potential vorticity conservation as a numerically independent method for checking a posteriori the dynamical consistency of an eddy-resolving GCM simulation. This is performed for a series of simulations with increasing horizontal and vertical resolution. The result that higher vertical modes play a catalytic role in the largest scales of eddy-driven flows is independently confirmed through this Lagrangian test.

1. Introduction

Recently, Barnier et al. (1991) raised the issue that the largest scales of eddy-resolving general circulation models (EGCM) were found to be rather sensitive to the spatial resolution used in both horizontal and vertical directions. The study was based on quasigeostrophic simulations of idealized double-gyre flows in a flat bottom, rectangular domain. A series of resolution tests were run, varying the horizontal grid size (either 20 km or 10 km) and the number of layers in the vertical (either 3 or 6 layers). The most striking result was that a major feature of the large-scale circulation, such as the zonal penetration of the midbasin inertial jet, increased by 40% when the horizontal grid size was halved for the six-layer experiments. The background stratification was kept identical for all cases and was chosen such that the radii of deformation were, respectively, about 40 km and 10 km for the first and fifth internal modes. All radii of deformation were therefore adequately resolved by the horizontal grid size for the highest three-dimensional resolution (six layers and 10-km grid size). In that simulation, the zonal jet length became at last rather insensitive to the value of the prescribed hyperviscosity coefficient: a change by a factor of 16 in hyperviscosity only induced a relative change of 7% in the jet length. For coarser resolutions, such a variation of hyperviscosity would cause a relative modification of the same order of magnitude in the penetration length. This insensitivity was suggestive of near numerical convergence for the largest scales of the circulation.

Because of the computer resources involved in these sensitivity tests (each of the high-resolution experiments requiring about 80 hours of cpu on a Cray-2), the purpose of this note is to explore alternate methods for checking the convergence of a simulation with respect to spatial resolution.

A proposed index for verifying a posteriori the three-dimensional consistency of the numerical solution is to check the conservation of potential vorticity along trajectories of Lagrangian particles. The method consists in seeding Lagrangian particles within the Eulerian evolving field and in checking if the computed trajectories are consistent with the implications of potential vorticity conservation. We show in this note that simulations corresponding to too coarse a 3D resolution [with either too few layers (e.g., 2 or 3) or a too large horizontal grid size (20 km)], fail to pass the test, while the conservation is verified overall for the six-layer and 10-km simulation.

The conservation of potential vorticity along Lagrangian trajectories has been originally examined by Haidvogel (1982, 1985) in models of two-dimensional turbulence on a β plane. His work provided evidence that the source of divergence between Eulerian and Lagrangian vorticity estimates lies in the aliasing errors involved in the nonlinear advection terms of the Eulerian field, while the interpolation error involved in the obtention of the trajectories remains negligible.

This conjecture is tested here in the context of *stratified* turbulent flows for the wind-driven double-gyre dynamics. The objective is to define simple consistency rules for the three-dimensional resolution, which is

Corresponding author address: Dr. Bach Lien Hua, IFREMER, B.P. 70, 29280, Plouzané, France.

© 1994 American Meteorological Society

necessary in numerical simulations including midlatitude eddies. The key idea is that the Eulerian and Lagrangian evaluations of changes in potential vorticity are numerically independent in their estimates of the *nonlinear advection* terms, in two-dimensional flows as well as in stratified flows.

Section 2 details the methodology used for float-tracking within the quasigeostrophic flow field. A special emphasis is put on the accuracy of schemes dealing with the Lagrangian dynamics, in order to use the error in Lagrangian potential vorticity conservation (LPVC), as a valid quantifier.

Section 2 reports on the influence of horizontal resolution of the Eulerian fields on the test of LPVC, by comparing results obtained in six-layer simulations for horizontal grid sizes of 10 and 20 km. It is noted that the vertical grid cell adequately resolves the angle of the baroclinic instability wedge, in the case of the highest resolution, suggesting a geometrical interpretation of a necessary three-dimensional resolution.

Section 3 addresses the issue of the vertical resolution necessary for stratified dynamics by intercomparing error levels in LPVC for a series of simulations with a 10-km grid size and with an increasing number of layers (two to six).

2. Determination of float trajectories

The method was originally proposed by Haidvogel (1982), and it is implemented using "particle-in-cell" ideas (Horowitz 1987) in order to vectorize the code over the number of floats. This enables the obtention of an efficient code for tracking Lagrangian particles, the Lagrangian computational effort representing a small overhead of the total cost. Typically, the tracking of 3000 floats per layer in the six-layer and 10-km case, represents an overhead of less than 20% in total cpu time. This large number of floats moreover allows enough degrees of freedom to compute statistics of the errors in LPVC.

The numerical method for the Eulerian part of the flow is documented in Barnier et al. (1991) and relies on the original code of Holland (1978). The potential vorticity conservation for a Lagrangian particle labeled m, within the kth layer is

$$\frac{d}{dt}(q_k^m(t)) = F_k^m(t) + D_k^m(t), \tag{1}$$

where the potential vorticity of particle m is

$$q_k^m(t) = \frac{f_0^2}{h_k}\left(\frac{\Psi_{k-1} - \Psi_k}{g'_k} - \frac{\Psi_k - \Psi_{k+1}}{g'_{k+1}}\right)(\mathbf{x}^m(t), t) + f_0 + \beta y(\mathbf{x}^m(t), t) + \Delta\Psi_k(\mathbf{x}^m(t), t) \tag{2}$$

and is the sum of the vortex stretching, planetary vorticity and relative vorticity, at the position $\mathbf{x}^m(t)$ of particle m, at time t. The depth of the kth layer is represented by h_k, f_0 is the Coriolis parameter, β is the meridional gradient of planetary vorticity, Ψ_k is the streamfunction in layer k, and g'_k is the reduced gravity jump at the interface between layers k and $k-1$.

The forcing and damping terms of (1) correspond to

$$F_k^m(t) = \delta_{k1}\frac{\mathrm{curl}\boldsymbol{\tau}(\mathbf{x}^m(t), t)}{h_1}, \tag{3}$$

$$D_k^m(t) = -A_4\nabla^6\Psi_k(\mathbf{x}^m(t), t) - \delta_{kN}r\nabla^2\Psi_k(\mathbf{x}^m(t), t), \tag{4}$$

where N represents the total number of layers, r the bottom friction coefficient, A_4 the biharmonic coefficient, and $\boldsymbol{\tau}$ the wind stress acting on the first layer.

Equation (1) is a simple ordinary differential equation that can be readily integrated along the particle trajectory (dropping the suffix for layer k):

$$q^m(t) - q^m(t_0) = \int_{t_0}^{t}\frac{d}{dt'}q^m(t')dt' = \int_{t_0}^{t}(D^m(t') + F^m(t'))dt'. \tag{5}$$

An important condition for obtaining an accurate integration of Eq. (1) is to compute a sufficiently accurate particle trajectory along which to integrate the right-hand side of Eq. (5) using a simple ordinary differential equation scheme. Note that the potential vorticity is conserved for all interior layers except for very weak dissipation due to hyperviscosity, while forcing and friction only act on the top and bottom layers.

The particle trajectory is obtained using a fourth-order Runge–Kutta procedure (dropping particle label m):

$$\frac{d}{dt}\mathbf{x} = \mathbf{v}(\mathbf{x}, t)$$
$$\mathbf{x} = (x, y)$$
$$\mathbf{v} = (u, v), \tag{6}$$

where successive time steps n and $n+1$ are such that

$$\mathbf{x}_{n+1} = \mathbf{x}_n + \frac{1}{6}\{\mathbf{k}_1 + 2\mathbf{k}_2 + 2\mathbf{k}_3 + \mathbf{k}_4\}, \tag{7}$$

and

$$\begin{cases} \mathbf{k}_1 = \delta t\mathbf{v}(\mathbf{x}_n, t_n) \\ \mathbf{k}_2 = \delta t\mathbf{v}\left(\mathbf{x}_n + \frac{1}{2}\mathbf{k}_1, t_n + \frac{1}{2}\delta t\right) \\ \mathbf{k}_3 = \delta t\mathbf{v}\left(\mathbf{x}_n + \frac{1}{2}\mathbf{k}_2, t_n + \frac{1}{2}\delta t\right) \\ \mathbf{k}_4 = \delta t\mathbf{v}(\mathbf{x}_n + \mathbf{k}_3, t_n + \delta t), \end{cases} \tag{8}$$

where δt is the time-step length. The velocity field at the particle position $\mathbf{x}$ is obtained by first fitting a stream

function field using a Lagrange interpolation over the 4×4 neighboring Eulerian grid points:

$$\Psi(x, y) = \sum_{i=1}^{4} \sum_{j=1}^{4} \Psi(x_i, y_j) \times \left[\frac{\prod_{\substack{p=1 \\ p\neq i}}^{4} (x - x_p) \prod_{\substack{q=1 \\ q\neq j}}^{4} (y - y_q)}{\prod_{\substack{p=1 \\ p\neq i}}^{4} (x_i - x_p) \prod_{\substack{q=1 \\ q\neq j}}^{4} (y_j - y_q)} \right]. \quad (9)$$

One can thus construct two independent expressions for the change of the particle potential vorticity. On the one hand, the Lagrangian estimate,

$$\delta q_L^m(t) = q(\mathbf{x}^m(t), t) - q(\mathbf{x}^m(t_0), t_0), \quad (10)$$

results from integrating the cumulative effects of the nonconservative processes along the Lagrangian trajectory. On the other hand the Eulerian expression,

$$\delta q_E^m(x, y, t) = \delta s^m(x, y, t) + \delta f^m(x, y, t) + \delta \omega^m(x, y, t) \quad (11)$$

is obtained by summing the changes in vortex stretching, planetary vorticity, and relative vorticity, computed at the instantaneous float position by interpolating the Eulerian fields, using the same Lagrange procedure as for the streamfunction field.

The dynamical consistency of the numerical simulation requires that these two estimates agree to some suitable accuracy and with sufficient three-dimensional resolution, the discrepancy should become arbitrarily small. Haidvogel (1985) discusses in detail the two sources of errors that can be identified, namely, (i) the Lagrangian interpolation errors and (ii) the truncation errors in the Eulerian flow fields, which cause aliasing effects in the nonlinear advection terms. Since the Lagrangian and Eulerian estimates differ in their treatment of the advective effects, it is granted that Eulerian aliasing effects can lead to large departures between the two estimates.

The Lagrangian interpolation error can be readily assessed by performing the test of releasing floats in frozen circulation fields (Lozier and Riser 1989) and calculating the rms departure of the particle's streamfunction from its initial value. After 100 days, the rms departure in the first layer remains less than 0.1% in all our cases, even for the coarsest three-dimensional resolutions. We shall see below that Eulerian truncation error levels can be dramatically larger, thereby exonerating the interpolation errors from being quantitatively important. Therefore, *the three-dimensional resolution of the eulerian flow is at the heart of the problem* and the next two sections document the respective role of horizontal and vertical resolutions in errors growth.

For a given layer, clusters of five particles are released in all cells of 100 km side within the southern half of the basin. Because of the north–south symmetry of the double-gyre problem, the study of the errors in LPVC in the southern half of the basin is adequate. The trajectories are computed for several independent time spans of 200 days and time series of Lagrangian and Eulerian changes of potential vorticity are accumulated for each particle trajectory. I have thus constructed datasets of the order of 10^6 (float $\times$ days) for each layer of each simulation.

The Lagrangian variability on the gyre-scale can be seen in Fig. 1, which displays a subsample of 200 days trajectories in the first layer of the highest resolution case H6-10 (see Table 1, which documents the parameters of the various runs). Only one out of every 25 trajectories of the full dataset is displayed in Fig. 1 in order to keep the legibility of the picture. A variety of patterns can be observed in the float trajectories: swift meandering paths along the inertial jet region, turbulent motions at the termination of the free jet and in the Recirculation region, circular motions of particles trapped within ringlike structures, motions akin to Rossby waves in the western and midbasin regions.

3. Influence of horizontal resolution

The full dataset has been analyzed by assessing the LPVC in all layers. We shall first examine the influence of horizontal resolution by comparing results obtained in the six-layer experiments with horizontal grid sizes of 10 and 20 km. The simulation with the coarser horizontal resolution is obtained by downgrading at a given initial time the 10-km Eulerian flow field onto a 20-

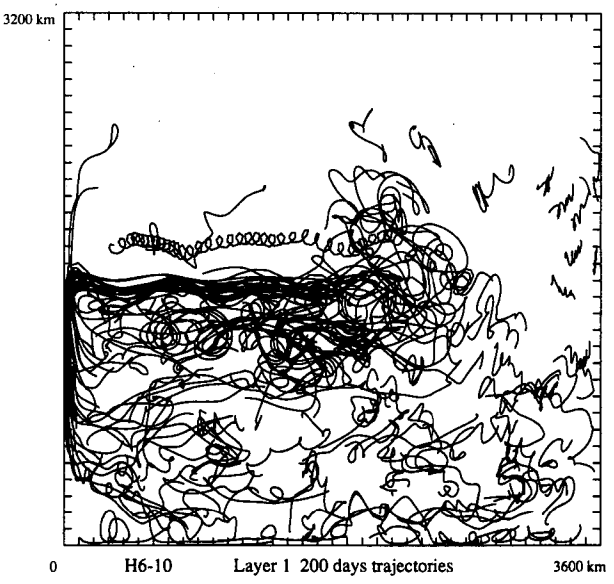

FIG. 1. Trajectories of a subsample of float trajectories in the first layer of simulation H6-10. The trajectories are plotted for the daily positions of the float while the actual trajectories correspond to a time step of 1 hour.

TABLE 1. Model parameters of all experiments. Basin size: 3600 km (zonal), 3200 km (meridional); Coriolis parameter: $f_0 = 9.3 \times 10^{-5}$ s^{-1}, $\beta = 2 \times 10^{-11}$ m^{-1} s^{-1}; steady wind stress: $\tau_0 = 0.60 \times 10^{-4}$ m^2 s^{-2}; bottom friction: $R = 10^{-7}$ s^{-1}; biharmonic friction: $A_4 = 4 \times 10^{10}$ m^4 s^{-1}.

Run	Number of layers	Δx (km)
L6-20	6	20
H6-10	6	10
H4-10	4	10
H3-10	3	10
H2-10	2	10

	Layer depths (m)	Reduced gravity (10^{-3} m s^{-2})	Radius of deformation (km)
H6-10	300, 350, 400, 500, 1350	12., 8.08, 5.24, 4.99, 1.17	38.8, 18.7, 12.6, 10.2, 9.2
L6-20	300, 350, 400, 500, 1350	12., 8.08, 5.24, 4.99, 1.17	38.8, 18.7, 12.6, 10.2, 9.2
H4-10	300, 450, 750, 3500	10., 8.02, 0.90	38.8, 18.7, 12.2
H3-10	300, 700, 4000	16.2, 14.3	38.8, 18.6
H2-10	300, 4700	0.0462	38.8

km grid and the same strategy for the seeding of floats is used. The integration of both Eulerian and Lagrangian variables is then pursued on the 20-km grid, keeping all external parameters identical.

a. Ensemble-averaged error

The overall degree of success in recovering potential vorticity balances in each layer can be captured through ensemble-averages of the rms differences between the Lagrangian and Eulerian estimates δq_L and δq_E:

$$r(\delta q)(t) = \langle (\delta q_E(t) - \delta q_L(t))^2 \rangle^{1/2}. \quad (12)$$

The results are summarized in Fig. 2 along with the observed changes in δq_L, which give the magnitude of the total dynamic range (Haidvogel 1985) experienced by the particles:

$$r(\delta q_L)(t) = \langle (\delta q_L(t) - \delta q_L(0)))^2 \rangle^{1/2}. \quad (13)$$

Similarly, the ensemble-average contributions of each component of potential vorticity, $r(\delta s)$, $r(\delta f)$, and $r(\delta\omega)$ can also be computed using analogous definitions and are also given in Fig. 2. Changes in potential vorticity have been scaled by β so that the ordinate axis is measured in kms of equivalent meridional displacement on a β plane.

The above procedure documents the growth of the various terms with time and reveals a tendency for saturation of variances after 30 days for run H6-10, at least in the first layer and bottom layer (this is slightly less clear for the middle layer 3). The saturation is observed earlier in time around day 15 in run L6-20. We shall therefore compare the results between the two experiments at both 15 and 30 days in order to characterize the ensemble statistics.

Levels of rms relative vorticity are of the same magnitude in both resolutions in all layers. One can construct a time scale from rms relative vorticity through a simple dimensional argument. Such an estimate would give a time scale of 1.5 days (resp. 3, 3) for layer 1 (resp. 3 and 6). In the context of homogeneous two-dimensional turbulence, Babiano et al. (1987) have documented through direct computations of absolute particle dispersion that the Lagrangian integral time scale, which measures the memory time scale of Lagrangian turbulence, is proportional to the inverse of rms relative vorticity. This time scale is significantly shorter than an Eulerian integral time scale, which is dominated by the time scale of energy-containing eddies. Such a concept might however not apply to the spatially inhomogeneous turbulent flow field of wind-driven gyres, where a large-scale shear flow exists. In such case, a dynamically relevant time scale is linked to the inverse of the meridional shear associated with the midlatitude surface jet: a variation of zonal velocity of 1 m s^{-1} across a meridional distance of 150 km (Barnier et al. 1991) leads to a shear time scale of about 2 days in the first layer. Values of 15 and 30 days at which error statistics are compared are therefore large enough when compared to the above time scales.

The major difference between L6-20 and H6-10 lies in the departures between the Lagrangian and Eulerian estimates observed in the coarse simulation, where the error $r(\delta q)$ becomes quite large very quickly after the initial launch time ($t > 1$ day). A fractional error defined as

$$\epsilon_1 = \frac{r(\delta q)}{r(\delta q_L)} \quad (14)$$

yields, respectively, 191% for L6-20 and 21% for H6-10 in the first layer at day 15. One could argue that because of internal anticorrelations between the components of potential vorticity, an alternate measure of fractional error (Haidvogel 1985), which is less stringent, could be to nondimensionalize $r(\delta q)$ by the rms relative vorticity, which clearly dominates the changes in potential vorticity in the first layer:

$$\epsilon_2 = \frac{r(\delta q)}{r(\delta\omega)}. \quad (15)$$

This yields 68% for L6-20 and 16% for H6-10.

The complete list of error statistics is given in Table 2a for the various layers at both 15 and 30 days. It is seen that throughout the whole water column, fractional errors ϵ_1 can approach or exceed 100% for the coarse resolution run while its largest value is of 27% for H6-10 after 30 days.

The observed improvement factor when the resolution is increased ranges from 4.6 to 9.1 for fractional error at various times. Such a value should be compared

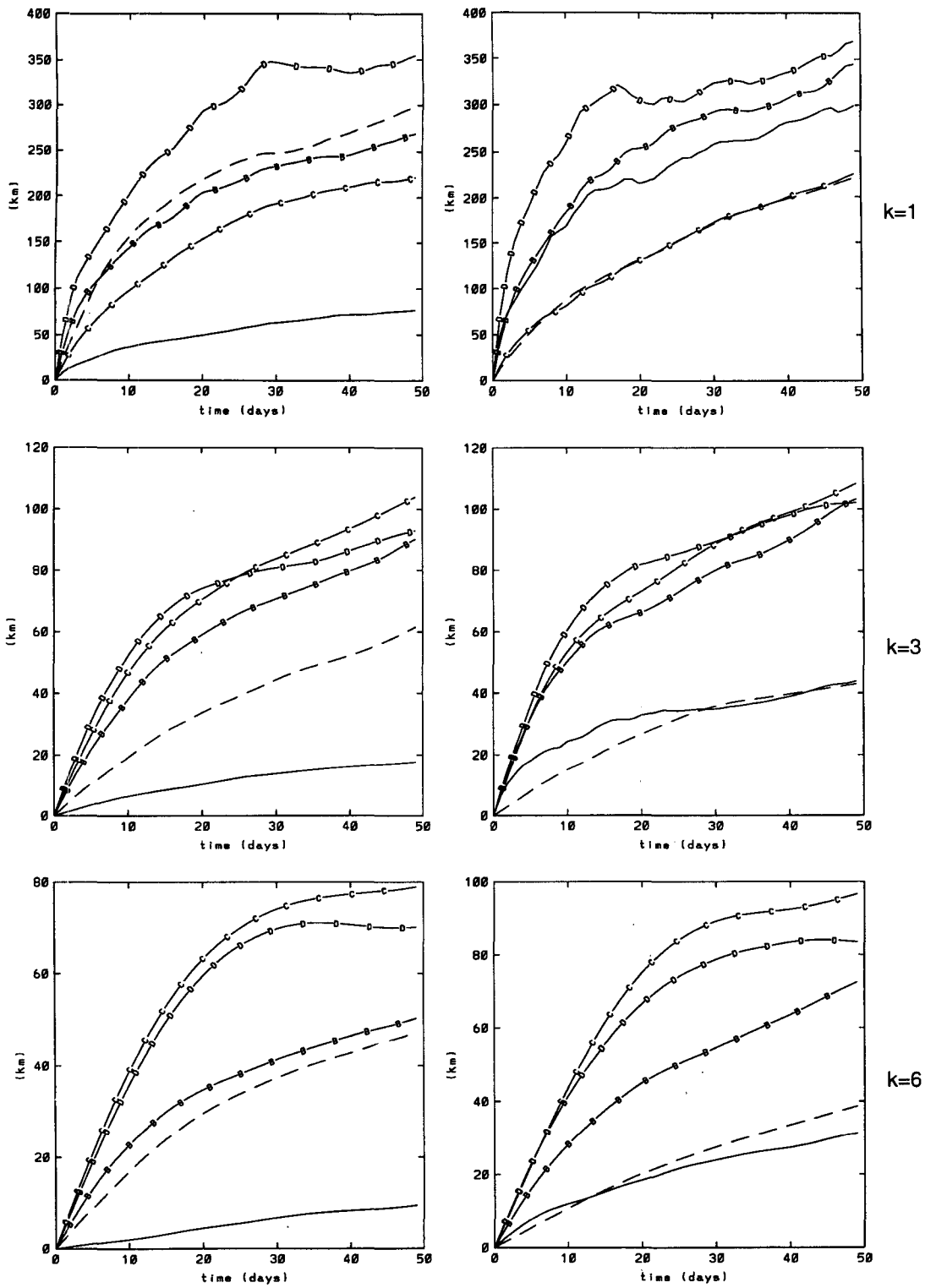

FIG. 2. Ensemble-averaged estimates of changes in potential vorticity for layers 1, 3, and 6 of runs L6-20 and H6-10: $r(\delta q)$ (solid), $r(\delta q_L)$ (dashed), $r(\delta s)$ (B), $r(\delta f)$ (C), and $r(\delta \omega)$ (D).

TABLE 2a. Fractional error ϵ_1 (in percentage) for run L6-20 and H6-10.

	t = 15 days				t = 30 days		
	$k=1$	$k=3$	$k=6$		$k=1$	$k=3$	$k=6$
L6-20	191	150	100	L6-20	114	126	88
H6-10	21	27	13	H6-10	24	27	19
Ratio	9.1	5.6	7.7	Ratio	4.8	4.6	4.6

with the increase by a factor of 8 of the computational effort necessary for the Eulerian flow field each time the horizontal grid size is halved, since the time step has to be reduced accordingly. Our results therefore indicate that the LPVC index follows closely the computational effort and we shall see below that this is also verified for the influence of vertical resolution. One is led to the conjecture that the accuracy of Lagrangian trajectories reflect the threefold accuracy in the two dimensions of horizontal space plus the dimension of time.

b. *Examples of LPVC*

Let us now examine particular examples of LPVC in the two simulations, which are chosen to illustrate the extremal error cases (either maximum or minimal) for the finest resolution simulation H6-10 and to document the generic patterns for error growths for the coarse resolution of L6-20.

Both Figs. 3a,b and Figs. 4a,b illustrate for both resolutions the vorticity balance and trajectory of a float initially launched in the first layer right at the separation point from the western boundary of the midlatitude. The figures display the time series of changes in potential vorticity for the Lagrangian estimate [label A, Eq. (10)] and Eulerian estimate [E = B + C + D, Eq. (11)], where components B, C, and D correspond, respectively, to vortex stretching, planetary vorticity, and relative vorticity. The fine-resolution solution statistically corresponds to a less convoluted jet with a longer zonal extension, while case L6-20 has typically a more meandering and shorter jet. The associated vorticity balance in case H6-10 illustrates the compensating effects of the changes in relative vorticity, vortex stretching, and slight meridional displacements associated with the jet meandering. A similar geographical release in the coarse simulation L6-20 (Figs. 4a,b) reveals that the Eulerian estimate is dominated by relative vorticity and departs at the end of the second meander quite rapidly from the Lagrangian estimate because of the dominance of relative vorticity.

The origin of the source of error for a given trajectory can be identified by the maximal covariance between the Eulerian estimate δq_L and a given component of potential vorticity. The covariance, which is an *absolute measure,* takes into account the component that has both the largest dynamical range and the largest correlation with the Eulerian aliased estimate. Such a measure is therefore quantitatively significant despite the existence of internal compensations between the components of potential vorticity.

Another example where the source of error is immediately apparent is given in Figs. 4c,d still for the coarse resolution case. The particle has been released in the first layer near the vicinity of the jet termination. In this case, vortex stretching displays the largest dynamical range and is clearly dominating the Eulerian estimate, causing its value to depart from the Lagrangian estimate. The last example for the fine-resolution case (Figs. 3c,d) corresponds to a particle trapped inside a ring, and the accurate vorticity balance is consistent with a tripartite exchange of potential vorticity.

c. *Baroclinic instability wedge*

One can raise the question of how to calibrate the horizontal resolution for a given vertical resolution. One obvious necessary condition is that sloping convective motions inside the baroclinic instability wedge of the mean flow (Pedlosky 1985) should be adequately represented by the elementary grid cells in the vertical plane. The wedge angle w corresponds to the angle between a mean isopycnal surface and the horizontal:

$$w = \left(\frac{\partial\bar{\rho}/\partial y}{\partial\bar{\rho}/\partial z}\right) = \left(\frac{f\bar{U}_z}{N^2(z)}\right),$$

$N(z)$ being the Brunt–Väisälä frequency. At a given level and for a given choice of layer depth Δz, the most sloping motion that the grid can accomodate corresponds to the shortest horizontal scale Δy and the associated angle of the isosurface is $\Delta z/\Delta y$. If the horizontal grid size Δy is such that the condition $\Delta z/\Delta y = Mw$, $M \ll 1$ is verified (e.g., for the case of a too large horizontal grid size), the discretized motions in the vertical plane are contrived to remain too flat for all scales such that $L > \Delta y$ and the entire span of the instability wedge cannot be covered. On the contrary, if the horizontal grid size is such that $M \gg 1$, then all horizontal scales L between $M\Delta y$ and Δy will be allowed to be slanted enough to experience baroclinic instability. Therefore a desirable condition corresponds to

$$\left(\frac{\Delta z}{\Delta y}\right)_{\min} \gg \left(\frac{f\bar{U}_z}{N^2(z)}\right)_{\max}. \tag{16}$$

In particular, this condition should be verified in the top layer where $\Delta z/\Delta y$ is minimal and $f\bar{U}_z$ is maximal. A rough estimate using the mean zonal velocity profile in the free jet region of simulation H6-10 yields for the uppermost layer,

$$w = \left(\frac{\partial\bar{\rho}/\partial y}{\partial\bar{\rho}/\partial z}\right) = 0.62\%.$$

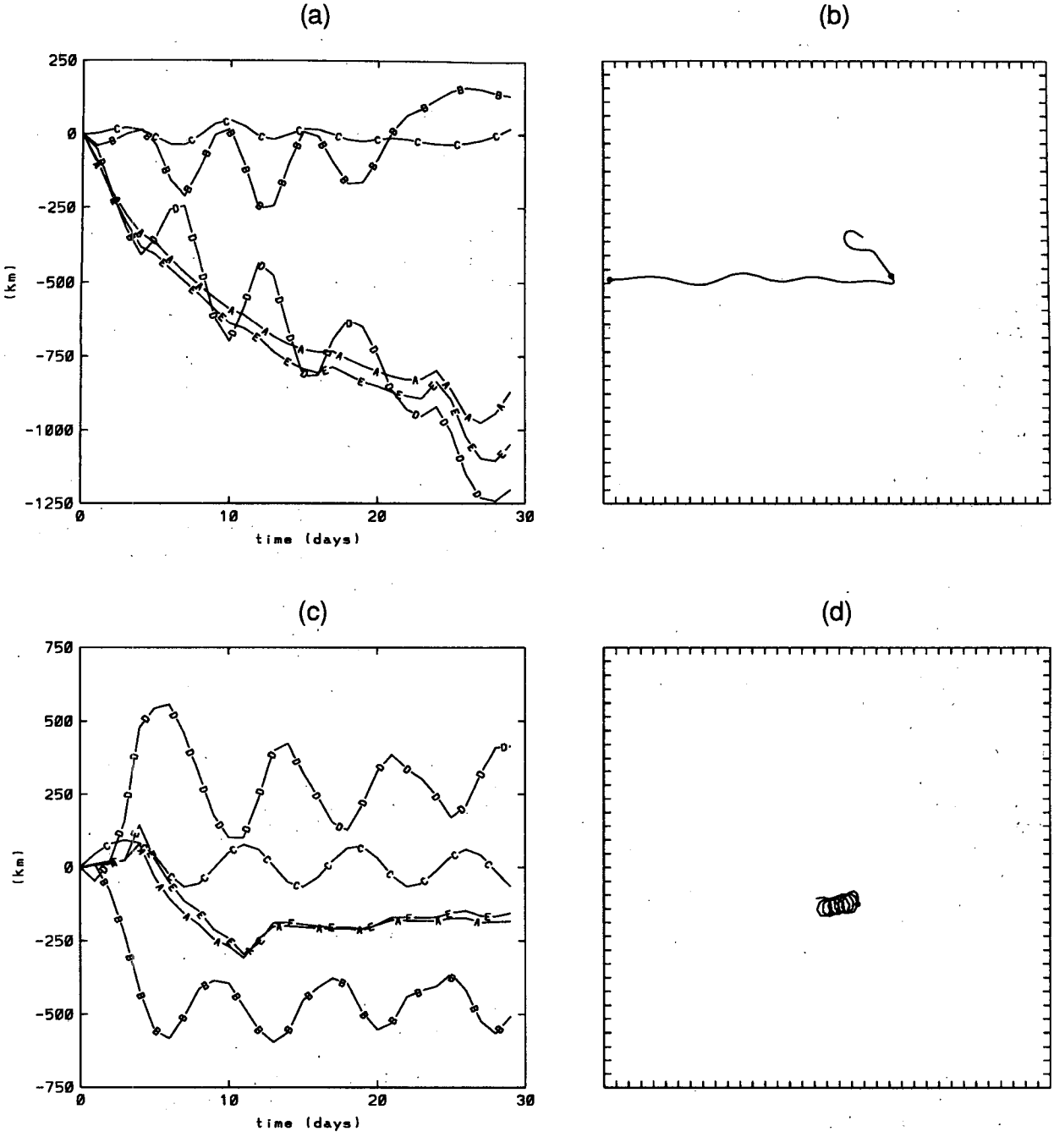

FIG. 3. (a) and (b) LPVC tests for a particle launched in the first layer of simulation H6-10 at the separation point of the midlatitude jet; A corresponds to the Lagrangian estimate of potential energy, E to the interpolated Eulerian value, and B, C, and D denote the vortex stretching and planetary and relative vorticities interpolated from the position of the particle on the Eulerian grid. The stars denote the initial particle position and its location 30 days after launch. The total length of the plotted trajectories is of 50 days. (c) and (d) Analogous plots for a particle trapped in a ring in simulation H6-10.

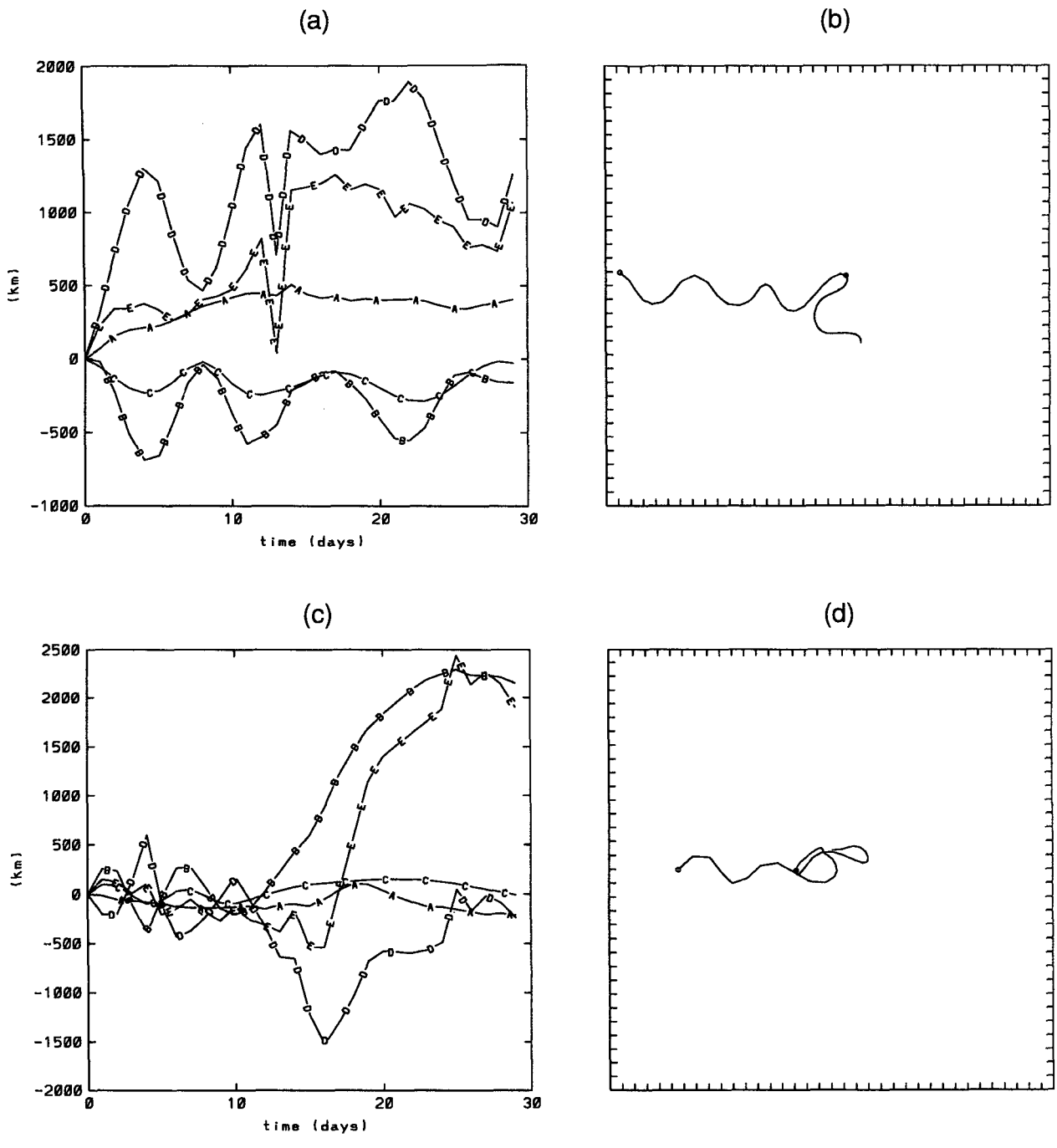

FIG. 4. (a) and (b) LPVC tests for a particle launched in the first layer of simulation L6-20 at the separation point of the midlatitude jet. The notations' conventions are identical to those of Fig. 3. Note the predominance of relative vorticity changes in the error. (c) and (d) Analogous plots for a particle that is caught in the termination area of the midlatitude jet.

For a grid size of 20 km, since $\Delta z = h_1 = 300$ m, we have $\Delta z/\Delta y = 2.4w$, which is marginally larger than w. For the 10 km grid size, we have $\Delta z/\Delta y = 4.8w$, which is sufficiently larger than w.

One could ask why a mere factor of 2 in the resolution of the instability wedge should lead to such a large improvement in the LPVC index. First it may be remarked that although we have considered the mean angle in the meridional direction only, in actuality the frontal jet area is contorted by meanders in both horizontal directions, so that the angle argument should also apply zonally to the instantaneous frontal feature in both directions. A general discussion of the applicability of this measure of the instability wedge angle to other classes of flows is beyond the scope of this note.

4. Influence of vertical resolution

To answer the question of how many layers should be kept, a series of simulations with a fine horizontal grid size of 10 km and an increasing number of layers (2, 3, 4) were compared to simulation H6-10. Table 1 documents the stratification parameters, which are such that resolved radii of deformation are identical to the lowest radii of H6-10. In all simulations, all radii of deformation are adequately represented by the 10-km grid, so that the only remaining possible sources of error are due to a lack of vertical resolution.

We shall restrict our study to the first layer since its depth is identical for all simulations. Ensemble-averaged errors of particle statistics within the whole southern basin show a substantial reduction in the fractional error ϵ_1 between the two-layer run and the rest of the 10-km experiments (Table 2b). There is, however, only a slight decrease in ϵ_1 between 3 and 6 layers (0.28 to 0.24). It may be noted that the two-layer configuration differs from the situation in the other experiments since there is no intermediate layer where neither forcing nor friction are active in this case. We have to resort to other types of statistics to discriminate more sharply the influence of vertical resolution for the experiments with $N \geq 3$. An alternate procedure for assessing errors is to focus on *maximal errors* that occur in the vicinity of the jet region, where the dynamics of the frontal feature are very sensitive to accurate vertical resolution. The inertial jet and its recirculation are characterized by large kinetic energy values, so that we have performed *conditional averaging statistics* on particle trajectories, sorting by instantaneous values of kinetic energy and geographical locations (in order to avoid the western boundary layer where velocities are also large). Such a procedure for error statistics remains therefore a purely Lagrangian method while it still enables one to focus on given geographical areas. The results of this conditional averaging are summarized in Table 2b and plotted in Figs. 5a–c. The three cases of Fig. 5 correspond to different sorting criteria, keeping only particles whose kinetic energy lies between the instantaneous maximal energy value and, respectively, one-fourth, one-third, and one-half that maximum. One can clearly identify a N^{-1} tendency (sketched by the continuous line) in the data points of conditional error, as the sorting retains only the particles with higher kinetic energy levels. Another conclusion that can be drawn is that, as for the case of ensemble-averaged index ϵ_1, the scaling of conditional error in N^{-1} suggests that the maximal LPVC error follows closely the total computational effort that is required for a given resolution. Indeed, the number of operations for the calculation of the Eulerian flow field increases roughly linearly with the number of layers.

TABLE 2b. Fractional and conditional maximal errors (in percentage) as a function of the number of layers for $t = 30$ days.

	ϵ_1	$\epsilon_{\max}^{(1/4)}$	$\epsilon_{\max}^{(1/3)}$	$\epsilon_{\max}^{(1/2)}$
H6-10	24	36	45	57
H4-10	24	43	54	65
H3-10	28	51	70	95
H2-10	44			

Although we have not done the actual numerical simulations, the above Lagrangian results suggest that the above LPVC maximal errors would still decrease if one continues to include more layers in the vertical. The trade-off is of course between a desired suitable accuracy and computing effort.

5. Conclusions

The resolution tests of Barnier et al. (1991) have been reexamined from a Lagrangian point of view by checking the conservation of potential vorticity along particle trajectories. We have found that both the ensemble-averaged and maximal LPVC errors are good global indexes for measuring the accuracy of a simulation, since they are directly linked to the overall computational effort required for the Eulerian flow fields. The Lagrangian errors therefore scale as p^{-3}, where p is the number of grid points in a given horizontal direction and as N^{-1}, where N is the number of layers.

Barnier et al. (1991) drew attention to the catalytic role played by the high vertical modes in EGCMs and to the fact that their small horizontal radii of deformation have to be resolved adequately by the horizontal grid size. Our Lagrangian error study quantifies the large role played by this horizontal resolution. The finest-resolution test, which corresponds to a configuration with six-layers and 10-km grid size, has fractional errors of less than 27% after more than 20 Lagrangian integral time scales and is therefore dynamically consistent from a Lagrangian point of view. This result concurs with the Eulerian indication of convergence

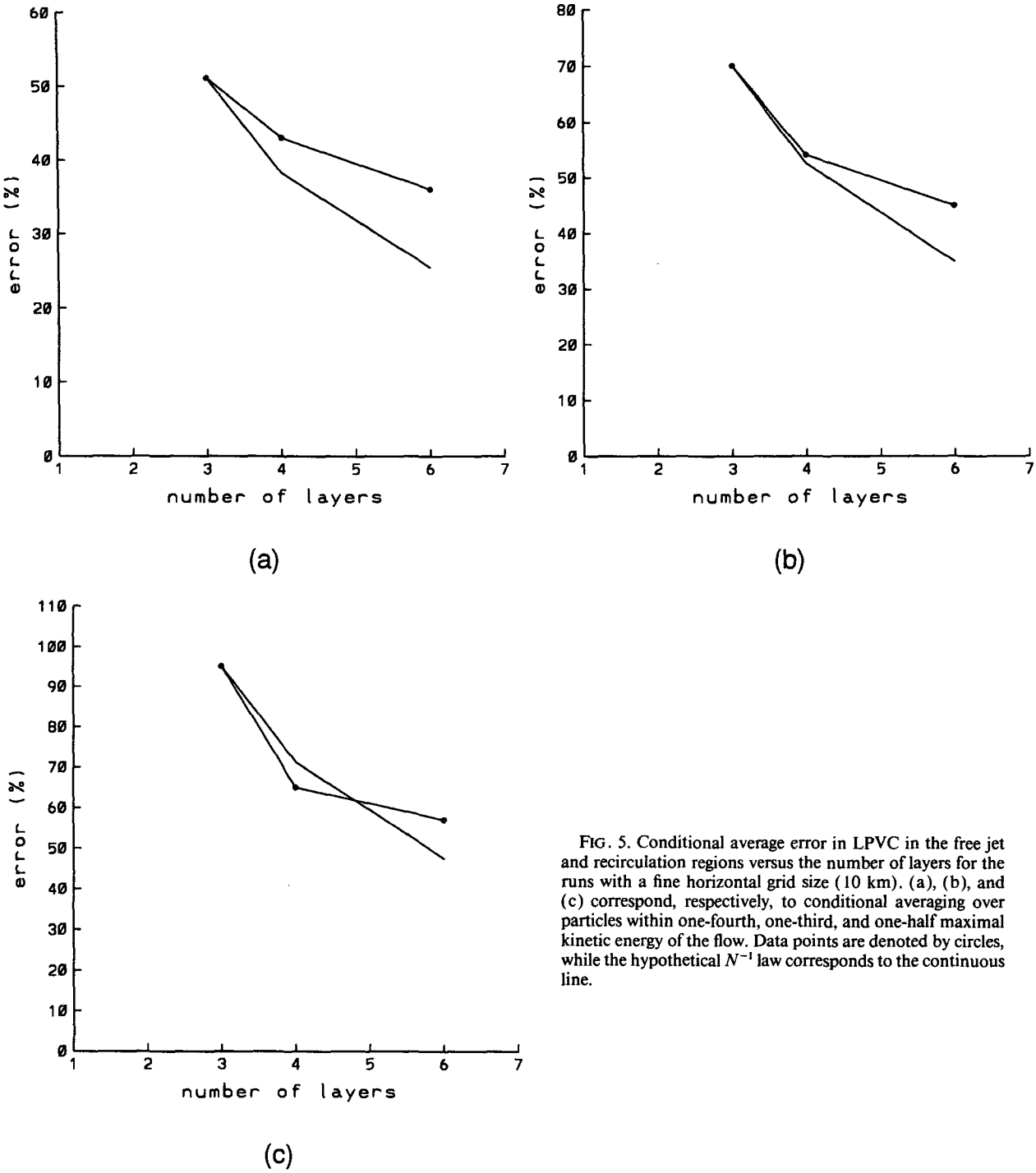

FIG. 5. Conditional average error in LPVC in the free jet and recirculation regions versus the number of layers for the runs with a fine horizontal grid size (10 km). (a), (b), and (c) correspond, respectively, to conditional averaging over particles within one-fourth, one-third, and one-half maximal kinetic energy of the flow. Data points are denoted by circles, while the hypothetical N^{-1} law corresponds to the continuous line.

with respect to values of the prescribed hyperviscosity, which has been reported in the Introduction. Lagrangian conservation tests should, therefore, be useful procedures for checking the degree of convergence of a stratified simulation since they have much less cpu-intensive requirements than Eulerian sensitivity tests.

Acknowledgments. Computing resources were provided at the CCVR (Centre de Calcul Vectoriel pour

la Recherche). I am indebted to Dr. D. Haidvogel for providing me with the float-tracking method and I would like to thank Drs. A. M. Treguier, S. Wacongne and P. Klein for their help during the process of writing up. Comments of the referees were helpful in improving the manuscript.

REFERENCES

Babiano A., C. Basdevant, P. LeRoy, and R. Sadourny, 1987: Single-particle dispersion, Lagrangian energy spectrum in two-dimensional incompressible turbulence. *J. Mar. Res.*, **45,** 107–131.

Barnier, B., B. L. Hua, and C. Leprovost, 1991: On the catalytic role of high baroclinic modes in eddy-driven large-scale circulations. *J. Phys. Oceanogr.*, **21,** 976–997.

Haidvogel, D. B., 1982: On the feasibility of particle tracking in Eulerian ocean models. *Ocean Modelling,* **45,** (Unpublished manuscript).

——, 1985: Particle dispersion and Lagrangian vorticity conservation in models of β-plane turbulence, (Unpublished manuscript).

Holland, W. R., 1978: The role of mesoscale eddies in the general circulation of the ocean. Numerical experiments using a wind-driven quasigeostrophic model. *J. Phys. Oceanogr.*, **8,** 363–392.

Horowitz, E. J., 1987: Vectorizing the interpolation routines of particle-in cell codes. *J. Comput. Phys.*, **68,** 56–65.

Lozier, M. S., and S. C. Riser, 1989: Potential vorticity dynamics of boundary currents in a quasi-geostrophic ocean. *J. Phys. Oceanogr.*, **19,** 1373–1396.

Pedlosky, J., 1987: *Geophysical Fluid Dynamics.* 2d ed. Springer-Verlag, 295 pp.